Multiscale chromatin dynamics and high entropy in plant iPSC cultures

Kinga Rutowicz[1], Joel Lüthi[2], Reinoud de Groot[2], René Holtackers[2], Yauhen Yakimovich[2], Diana M. Pazmiño[1], Olivier Gandrillon[3], Lucas Pelkmans[2] and Célia Baroux[1]

[1] *University of Zurich, Institute of Plant and Microbial Biology, Plant Developmental Genetics, Switzerland*

[2] *University of Zurich, Department of Molecular Life Sciences, Switzerland*

[3] *University of Lyon, ENC de Lyon, Laboratory of Biology and Modeling of the Cell, France*

Keywords

Arabidopsis, iPSC, protoplast, chromatin dynamics, nuclear morphology, texture features, H1, linker histone, H2B, high-throughput imaging, high content imaging, supervised image analysis, entropy, cell-to-cell variability

Abstract

Protoplasts, derived from plant tissues, are considered functional equivalent of animal induced pluripotent stem cells (iPSC). Similarly, to their animal counterparts, plant iPSC show large-scale, chromatin reorganisation, thought to be a hallmark of pluripotency acquisition. To capture in more details the nuclear morphology and chromatin organisation of plant iPSC, we deployed high-throughput imaging and a custom, supervised image analysis protocol extracting over 100 chromatin features. Our study unravels a rapid, multiscale dynamics of chromatin patterns which trajectory strongly depends on nutrients availability. We measured a high heterogeneity of chromatin features indicating an intrinsic entropy of iPSC cultures, which reduced over time. We found that entropy reduction is antagonistically controlled by phytohormones and intrinsic epigenetic factors.

Introduction

Plant tissues have a remarkable plasticity. This phenomenon is illustrated by the capacity of plant parts, tissue fragments or isolated cells *in vitro* to regenerate whole plant individuals. This property is largely exploited by horticulture and agriculture since centuries for the accelerated amplification of garden plants, crop and tree species, the propagation of disease-free plants, the production of plant biomass for industrial applications and the creation of starting material for genetic engineering approaches (Ibanez et al., 2020; Ikeuchi et al., 2019; Reed & Bargmann, 2021; *Special Issue "New Frontiers in Micropropagation"*, 2021). By contrast, organ regeneration, notably from single cells, is not a prevalent property in the animal kingdom, except in basal lineages like in Cnidarians (Holstein et al., 2003).

Cellular plasticity describes the ability of differentiated cells under certain conditions to reprogramme physiologically and molecularly towards a pluri-competent (or pluripotent) state (Reddy et al., 2021). There is a vivid interest in understanding the mechanisms controlling cellular plasticity. In animals, several pioneer transcription factors have been identified that can potentiate cell reprogramming following overexpression *in vitro* (Iwafuchi-Doi & Zaret, 2014). Similarly, several transcription factors were identified in the model plant Arabidopsis that share tissue reprogramming properties (BABYBOOM, WUSCHEL, LEAFY COTYLEDON1, WOUND INDUCIBLE 1 (reviewed in (Ikeuchi et al., 2019; Iwase et al., 2017; Iwase et al., 2011)) of which so far only LEAFY was formally demonstrated to share the molecular and cellular properties of a pioneer transcription factor (Jin et al., 2021). In addition, several studies concur to the idea that chromatin modifiers, controlling the epigenetic landscape and accessibility, are key to cellular plasticity, in both plants and animals (Birnbaum & Roudier, 2017; Reddy et al., 2021). For instance in Arabidopsis, mutants with reduced levels of DNA methylation or histone methylation (particularly H3K4me4, H3K27me3, and H3K9me2) have altered plasticity and are impaired, or, by contrast enhanced abilities for somatic embryogenesis, callus production, shoot or root regeneration or a combination thereof (He et al., 2012; Ishihara et al., 2019; Jing et al., 2020; Lee & Seo, 2018; Reddy et al., 2021; Shemer et al., 2015).

Conveniently, plant cells from differentiated tissues can be induced *in vitro* to become pluripotent, by simply releasing them in culture following an enzymatic degradation of their cell wall (reviewed in (Muller-Xing & Xing, 2022)). When cultivated on medium supplemented with phytohormones, these protoplast cells can proliferate to form microcalli, some of which will further differentiate into shoot and root tissues, to eventually form a fully fertile plant. For this reason, protoplasts are considered induced pluripotent cells conceptually similar to animal induced pluripotent stem cells

(iPSCs) (Grafi et al., 2011; Sang et al., 2018), and will therefore be referred thereafter as plant iPSC.

The release of plant iPSC rapidly leads to transcriptome reprogramming with a large fraction of genes corresponding to stress responses, energy metabolism and photosynthesis (Chupeau et al., 2013). But this response is not uniform, even in nearly pure iPSC cultures derived at 95% of mesophyll cells and display a high level of heterogeneity in the transcript composition among cells (Xu et al., 2021). This is accompanied by profound changes in chromatin organisation including a broad increase in chromatin accessibility (Xu et al., 2021; Zhao et al., 2001) and in histone acetylation, thought to establish a transcriptionally permissive landscape (Williams et al., 2003). Chromatin changes are also visible at the cytological level. Pioneer studies in tobacco iPSC then Arabidopsis (Tessadori et al., 2007; Williams et al., 2003; Zhao et al., 2001) showed that the chromatin of leaf-derived iPSC is rapidly reorganised after release. Typically, heterochromatin decondenses during, or shortly after isolation (Zhao et al., 2001), leading to the spatial dispersion of centromeric and pericentromeric repeats together with their associated DNA and histone methylation marks (Tessadori et al., 2007) and decondensation of rDNA arrays (Ondrej et al., 2010). Despite these large-scale alteration, transposable elements and genomic repeats remain transcriptionally silent, suggesting uncoupling of heterochromatin condensation and silencing (Tessadori et al., 2007). Within the first 3-5 days of iPSC culture, heterochromatin gradually recondense and the transcriptome changes again for more attributes of the cell cycle and regeneration process (Chupeau et al., 2013; Xu et al., 2021).

With the aim to have a comprehensive, quantitative overview of the cytological patterns of chromatin (re)organisation we used high-throughput imaging and customised a supervised-learning image processing to analyse Arabidopsis iPSC within the first 5-7 days of culture. Multivariate analysis of the different chromatin features revealed rapid chromatin changes following leaf iPSC release at different scales. iPSC chromatin also changed in composition, with a notable decrease in linker histone complements. We found that the trajectory of chromatin changes largely depends on nutrient availability but less on phytohormones. In addition, leaf iPSC cultures, although derived principally from mesophyll cells, are characterized by a high heterogeneity as assessed by entropy of chromatin patterns which decreases progressively in the following 5-to-7 days. Finally, we found that entropy reduction is dampened in the absence of phytohormones but enhanced by an inhibitor of histone deacetylation.

Results

H1 as a marker of chromatin reorganisation in iPSCs.

To select a live reporter monitoring chromatin changes in Arabidopsis leaf iPSC cultures we analysed various, fluorescently tagged, core and linker histone variants. First, we considered the three Arabidopsis linker histone variants for which translational fusions are available (Rutowicz et al., 2019; Rutowicz et al., 2015). In a first approach, we scored the number of fluorescent positive cells at day 0 (just after isolation), at day 2 and at day 5. At day 0, H1.1-RFP and H1.2-GFP were detected in most cells (96%, n= 138 and 75%, n= 168, respectively). But at day 5 the fraction of detectable, positive cells had decreased by ~25% and 22%, respectively (**Figure 1A-B, Supplemental Figure 1A**). By contrast, the stress inducible, H1.3-GFP variant reporter was detected only in 2% cells at day 0, likely corresponding to guard cells in which it is constantly expressed (Rutowicz et al., 2015). This fraction did not increase upon culturing (**Figure 1C, Supplemental Figure 1A**). Thus, this marker was not further considered. In a second approach, we focused on H1.2 which is the most abundant variant in leaf cells (Kotlinski et al., 2016) and quantified the mean signal intensity per nucleus. We measured a 30% decrease of H1.2-GFP abundance in the fraction of expressing nuclei at day 5 (**Figure 1D**).

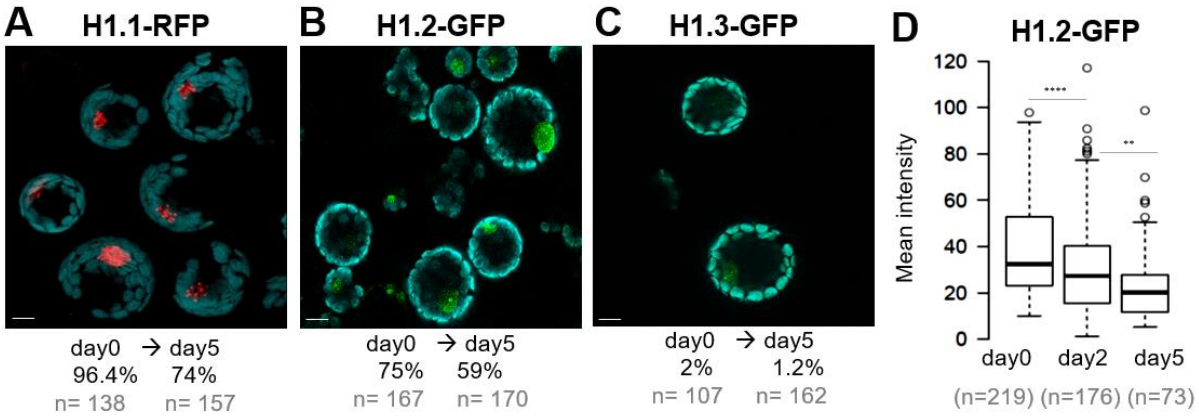

Figure 1. The establishment of plant iPSC cultures is marked by a decreasing abundance in H1.1 and H1.2 linker histone variants.
Leaf-prepared, induced pluripotent plant cells (iPSC) expressing fluorescently tagged variants of H1.1 (A), H1.2 (B) and H1.3 (C) were followed for five days in culture. (**A-C**) Representative images and % of cells showing detectable fluorescence (n= number of cells scored). See also graphs in Supplemental Figure 1. Cyan - chloroplasts (autofluorescence), red – RFP, green – GFP. (**D**) measurements of H1.2-GFP signal intensity in a replicate culture sampled at day 0, 2 and 5. ***, P<0.001 ; **, P<0.01 (Mann-Whitney-U test). Scale bar 10 µm

In contrast, two core nucleosome histone reporters (pUBI10::H2B-RFP and pHTR5::HTR5-GFP abbreviated H2B-RFP and H3.3-GFP, respectively) were equally detected throughout culturing time (**Supplemental Figure 1B**). A tagged H2A.Z reporter also included in the analysis was not further considered since it captured only ~40% cells (**Supplemental Figure 1B**).

Finally, to quantify the mitotic competence of the iPSC cultures in our conditions, we monitored the S/early G2 phase H3.1-mCherry marker (Desvoyes et al., 2020). At day 0 only 5% cells (n=275) showed detectable signal increasing to 8% (n=250) at day 5 and 11% (n=230) at day 6 (**Supplemental Figure 1C**). Thus, iPSC cultures are mitotically relatively quiescent in the first 6 days and the rarity of S-phase cannot explain the broad decrease in H1 abundance in iPSCs occurring already at day 2.

A semi-automated pipeline for high-throughput analysis of chromatin reporters in iPSC.

We aimed at high-throughput imaging of plant iPSC in culture, similar than done previously for analysing cellular morphology (Dawson et al., 2022), but focusing here on chromatin markers. For this, we generated a dual reporter Arabidopsis line expressing both the H1.2-GFP and H2B-RFP markers mentioned above, that we used to establish and benchmark the growth conditions, imaging setup and an image analysis pipeline. The details are provided in the Methods but in short, iPSCs produced from young leaves were cultured under sterile conditions in coverglass-bottom 96-well plates for semi-automated imaging using Cell Voyager (**Figure 2A**). The imaging set-up allows to capture up to 60 wells*, i.e.* 60 cultures, per multi-well plate, each being covered by 6 region-of-interest (ROIs). Imaging of a full 60x6 ROIs takes 90 min. After each time point, the plate was returned to the temperature and light-controlled plant growth incubator until the next measurement. Image analysis, illustrated in **Figure 2B**, consisted in a supervised, batch processing approach comprising the following steps performed in TissueMaps (http://tissuemaps.org): (i) maximum intensity projection of the image series; (ii) denoising; (iii) watershed-based segmentation of H2B-RFP-stained nuclei and image masking using the segmented objects; (iv) training, classification and filtering of segmented objects to improve nuclei segmentation; (v) quantitative measurements using validated nuclei objects.

To benchmark this approach, we cultured iPSC expressing the dual marker in replicate wells and applied our imaging and image processing procedure between day 0 and day 7 (representative images **Supplemental Figure 2A-B**). The setup of replicate wells allowed to capture a total of 500-1000 nuclei per time point, per initial culture. Using FDA staining (Saruyama et al., 2013) we confirmed a high density of viable cells at each time points (**Supplemental Figure 2C**). However, we observed a decrease in the number of nuclei (cells) identified following the segmentation, particularly at day 7 (**Supplemental Figure 2D**), indicating loss of viability, and consistently with previous reports (Chupeau et al., 2013; Xu et al., 2021). The analysis of GFP to RFP ratios per nuclei confirmed a dramatic reduction of H1.2 abundance relative to H2B in iPSCs as soon as day 3 (**Figure 2C**). This automated measurement compared very well to a set of manually segmented

images used for the same intensity ratio measurement (**Figure 2D**). Then, to assess the reproducibility of the culturing-imaging-image analysis workflow, we set up eight replicate measurements in the same multiwell plate with iPSC from two independent reporter lines expressing H1.2-GFP and H2B-RFP. The H1.2-GFP/H2B-RFP intensity ratio distributions were highly consistent between wells at each day (**Supplemental Figure 2E**). Finally, as a control, we analysed iPSCs co-expressing a nuclear localised (nls)-YFP and the same H2B-RFP internal control, using the same setup as before. The analysis showed a stable ratio during culturing (**Figure 2E, Supplemental Figure 2F**).

In conclusion, we have established a robust automated high-throughput imaging-image analysis workflow enabling the automated capture of several hundred nuclei in iPSC cultures per time point suitable for quantitative measurements. In addition, the quantifications showed that the decrease in H1.2 abundance is a hallmark of chromatin changes within the first two days after iPSC release.

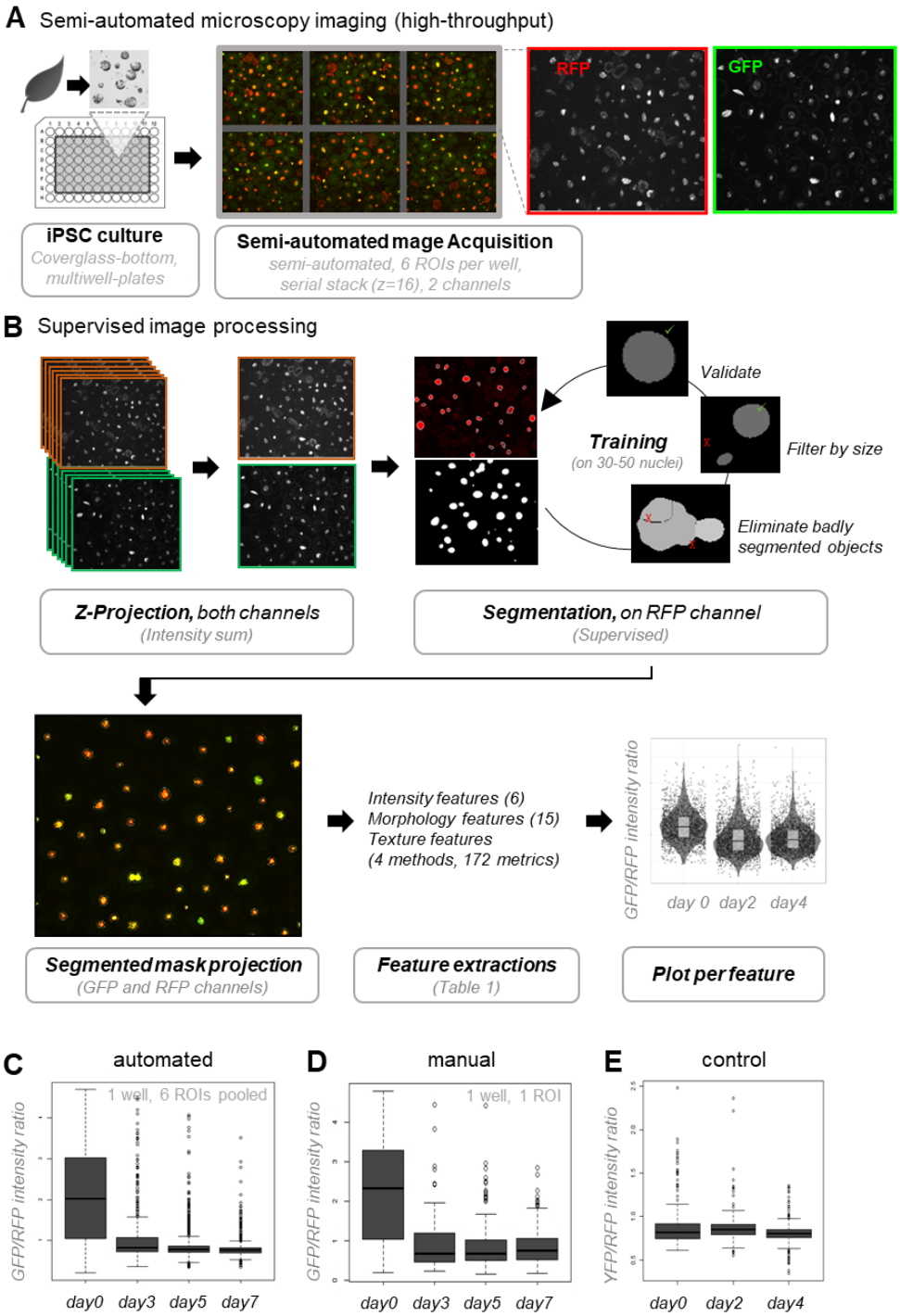

Figure 2. A semi-automated pipeline for high-throughput analysis of chromatin reporters in Arabidopsis iPSC cultures. (**A**) Semi-automated microscopy imaging is caried out in cover-glass bottom multi-well plates using a Cell Voyager platform. Six Regions of Interest (ROI) are randomly selected per well and imaged for each channel. The procedure is repeated for each time point, the culture being returned to the growth incubator in between two measurements (**B**) Supervised image processing following a workflow as depicted was applied using TissueMaps (www.tissuemaps.org) and enabled the segmentation of several hundred nuclei with high accuracy. The image analysis package returns several descriptors (features) of the segmented objects describing the morphology, the intensity distribution and texture (see details in the text). These metrics can be plotted or further analysed. (**C-D**) Comparison of the H1.2-GFP/H2B-H2B ratios obtained following automated (C) or manual (D) image analysis, showing a reproducible reduction of H1.2-GFP relative to H2B-RFP during culturing time (experiment HTI001). (**E**) Control experiment showing stable signals of a nuclear localised, free YFP marker, relative to H2B-RFP levels (experiment HTI002).

Nuclei morphology and chromatin patterns change rapidly after iPSC release.

Next, we exploited the numerous image features exported by the pipeline to analyse the cytological organisation of chromatin in iPSC, particularly during the first days of culturing, before the cells start dividing. Three groups of metrics were produced from the analysis: signal intensity features, morphology features and texture features. This corresponds to a total of 193 metrics per channel and 370 for both channels (morphology features were derived from segmentation on the H2B-RFP signal only, Table1). A principal component analysis (PCA, (Metsalu & Vilo, 2015)) that included all the features indicated clear changes within the first two days of culturing time (**Figure 3A,** replicate **Supplemental Figure 3A**).

To then estimate the contribution of each feature groups we carried out separate PCA. Clearly, each of the intensity, morphology and texture features contributed to explain chromatin organisation changes in iPSC (**Figure 3B-D**, **Supplemental Figure 3A**).

The observation that intensity features separate the iPSC from day 0 and day 2, day 5 indicate that the relationships between chromatin markers change rapidly. Consistent with our previous observation that iPSCs barely divide within the first 5 days of culturing, we found that H2B-RFP intensity distribution did not significantly change during this period of time, but increased, however, at day 7 probably indicating that cells entered S phase (**Supplemental Figure 3B**). Likely, the global decrease in linker histone abundance (H1.2-GFP), relative to total chromatin (H2B-RFP), documented before, largely contribute to separate iPSC on the PCA. Yet, the standard deviation, min and max intensity values also contribute the principal components (**Supplemental Figure 3C**) suggesting that, beyond the absolute levels of chromatin markers, their distribution, reflecting the occurrence of chromatin regions with varying density, also change rapidly.

Morphology features are computed on the segmented H2B-RFP signal, thus provide a proxy for nuclei size and shape (**Supplemental Figure 3D**). A PCA considering all morphology features indicated that nuclei undergo continuous size and shape changes between day 0 and day 5 (**Figure 3C, 3E**). Interestingly, although an increase in nuclear size would be expected from the decreased abundance in H1 variants (Rutowicz et al., 2019; She et al., 2013) we did not detect a positive correlation, albeit a moderate one at day 5 (Pearson correlation $r < 0.3$, **Supplemental Figure 3E**). Instead, the size distribution of iPSC nuclei shifts towards smaller sizes at day 2 and day 5 (**Supplemental Figure 3F**). The median and the distribution of shape descriptors of iPSC nuclei at day 5 also differ from day 0 (**Figure 3E**), with, for instance, slightly rounder and less elongated nuclei at day 5 than day 0 (**Figure 3F**).

Next, we interrogated the group of texture features, showing a clear evolution during culturing (**Figure 3D**). Textures metrics describe the spatial distribution of signal intensities as a function of

scale (Depeursinge et al., 2017a; Di Cataldo & Ficarra, 2017) and can be used to analyse patterns in chromatin organisation (Kerr et al., 2010; Lee et al., 2021; P. Rana et al., 2021). TissueMaps returns metrics corresponding to four types of texture analysis: Gabor wavelet filter, Local Binary Pattern (LBP), Threshold Applied Statistics (TAS), and Hu invariant moment (Hu) (reviewed in (Di Cataldo & Ficarra, 2017), (Hamilton et al., 2007); list Table 1). The LBP analysis, based on neighbouring pixel intensity scanning in incrementally growing circles, is particularly interesting as a proxy of chromatin organisation patterns at different length scales (**Supplemental Figure 3G**) (Di Cataldo & Ficarra, 2017; P. Rana et al., 2021). We detected a rapid, global decrease in LBP values along the different radii for the H2B-RFP signal (**Figure 3G**) suggesting a decreasing heterogeneity in chromatin distribution at day 2. The texture metrics of H1.2-GFP signal also showed rapid changes in iPSC chromatin (**Supplemental Figure 3G**). These dynamics in H2B-RFP and H1.2-GFP textures, reflecting the distribution pattern of these histone variants, were confirmed with the TAS and Gabor filter methods (**Supplemental Figure 3H-I**). Furthermore, we detected modest, but consistent positive correlations between the LBP metrics and the H1.2-GFP / H2B-RFP ratio, indicating that the changes in chromatin distribution patterns are likely linked with the relative abundance of linker and nucleosome histones (**Supplemental Figure 3J**).

Collectively, the analysis of nuclei morphology and of H2B-RFP signal distribution indicate clear changes in nuclear size, shape and in chromatin organisation in freshly released iPSC. These changes occur largely within the first two days of plant iPSC cultures and are concurrent, but not correlated, with a decrease in the relative abundance of linker histone H1.2. The distinct texture of H2B-RFP distribution at different length scales at day 5 compared to day 0 suggests a reorganisation of chromatin domains at the (sub)micrometre scale.

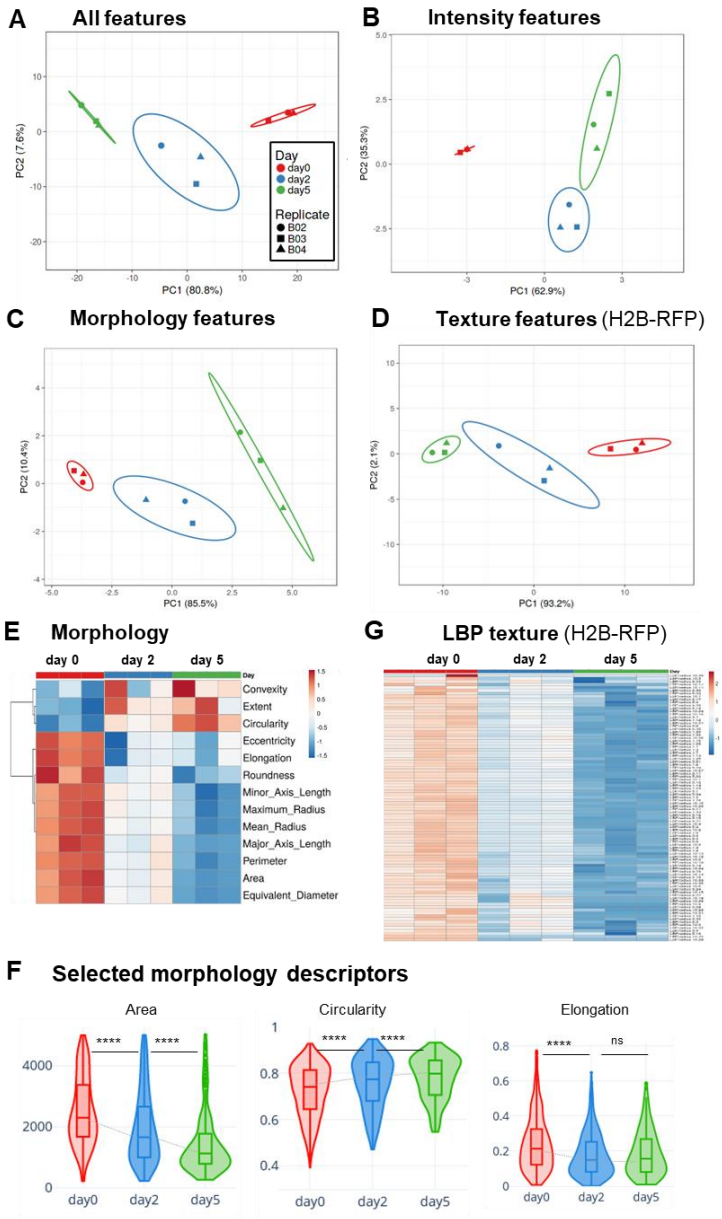

Figure 3. Marked changes in nuclear morphology and chromatin organisation in iPSC cultures

(**A-D**) Principal Component Analysis (PCA) of chromatin features measured in iPSC expressing H1.2-GFP and H2B-GFP, imaged ~4h after release (day0), at day 2 and day 5 (experiment HTI004). (A) PCA computed on all features (see list Table 1), (B) PCA on H1.2-GFP and H2B-GFP intensity features, (C) PCA on morphology features, *i.e.* size and shape descriptors of the segmented nuclei, (D) PCA on LBP texture features for H2B-RFP. See also Supplemental Figure 3A for replicate PCAs, Supplemental Figure 3B for the PCA loading scores per descriptors. X and Y axis show principal component 1 and principal component 2 that explain the given % of the total variance, respectively. Ellipses: 95% confidence interval. Each point represents a culture replicate (well). (**E)** Relative changes for each morphology descriptors during culturing. Heatmaps represent the median value for each descriptor, with unit variance scaling applied to rows. (**F**) Plots of selected morphology descriptors. (**G**) Relative changes for LBP texture descriptors for the H2B-RFP signal distribution. Heatmaps represent the median value for each descriptor, with unit variance scaling applied to rows. Number of nuclei, n= 1008, 508, 238 at day 0, 3, 5 , respectively. ****, p<0.0001; ns, not significant, Kruskal Wallis test followed by post-hoc Dunn's test and Bonferroni correction.

Plant iPSC cultures show a marked heterogeneity in their chromatin features, which reduces over time.

The former analysis clearly showed spread distribution of intensity, size and shape descriptors, indicative of a vast heterogeneity of nuclei type, despite the fact that leaf-derived iPSC consist in ~85-90% mesophyll cells (Xu et al., 2021). To assess this heterogeneity, we first generated density distribution maps of iPSC chromatin features summarised by the principal components computed previously. The maps confirmed a broad dispersion of the data in the PC landscape, indicating a very heterogenous population in terms of nuclei type and chromatin patterns (**Figure 4A**). The distribution however changed over time with an apparent enrichment of nuclei with similar PC values at day 5 (**Figure 4A and Supplemental Figure 4**).

To quantify this heterogeneity and possible changes during the culturing time, we computed the entropy of the data. Entropy is a useful measure of variability in biological data, capturing both the variance and the shape of the data distribution (Gandrillon et al., 2021). The analysis indeed revealed a marked positive entropy (H_0) for a large fraction of chromatin features (**Supplemental Figure 4B**), changing significantly over time.

We then analysed the family of features separately and found that heterogeneity as assessed by a positive entropy was contributed by all features (**Figure 4B**). Strikingly, the entropy decreased over time, particularly that of texture features and moderately for morphology features, while it remained largely positive for intensity features. Interestingly, the heterogeneity of chromatin distribution, measured by LBP texture features on H2B-RFP, was higher at a small length scale (LBP radius 1, **Supplemental Figure 4C**) but entropy reduction over time (ΔH_0) was more significant for the highest length scale (radius 10, **Figure 4C**).

These findings were confirmed in a replicate experiment and where an additional imaging time point, at day 7 showed that entropy continue to decrease but more slowly after day 5 (**Supplemental Figure 4D**).

In conclusion, entropy analysis of the date indicates a profound heterogeneity of nuclei morphology and of chromatin organisation in freshly released iPSC. Strikingly, heterogeneity reduces progressively, mostly within the first five days, and more particularly for chromatin distribution patterns (texture). This suggests a tendency towards homogenisation of chromatin types, although entropy remains high even after 7 days.

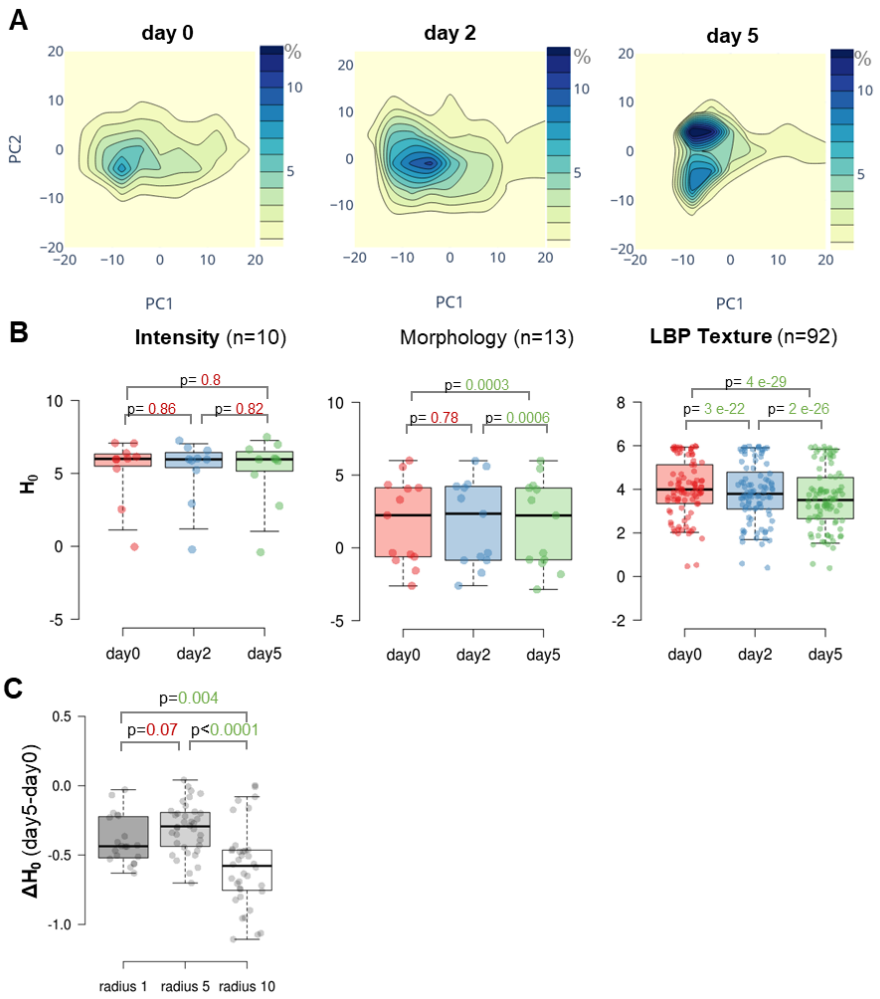

Figure 4. Plant iPSC cultures are characterized by high entropy of chromatin features, reducing over time.

(**A**) Density distribution of chromatin features summarised by principal components PC1 and PC2 as computed in Figure 3A. Density contours are coloured according to the frequency (percent) of nuclei falling in the corresponding PC space. (**B**) Entropy (H_0) of chromatin features per family (n, number of descriptors per family). (C) Differential entropy (ΔH_0) between day 5 and day 0 for LBP texture features of H2B-RFP and at different length scale (radius). P values, paired Wilcoxon rank test. Data for all plots in Figure 4 come from the experiment HTI004.

Chromatin heterogeneity in iPSC is influenced by phytohormones.

Arabidopsis leaf iPSC cultured in the absence of phytohormones do not grow nor divide and undergo progressive cell death (Zhao et al., 2001). We thus asked whether the chromatin changes quantified within the first days of iPSC culturing are part of the cellular responses to phytohormones. For this, we partitioned the initial pool of freshly released iPSC in two media: either in the regular Gamborg B5's medium (Gamborg et al., 1968) rich in macro- and microelements, vitamins, supplemented with glucose (2%) and phytohormones (auxins and cytokinin); or in the same medium but without phytohormones. First, we asked whether the absence of phytohormones would affect the reduction in the relative abundance of linker histones

(H1.2) that was observed previously. Quantifications showed that this is not the case and H1.2 reduction is still taking place in the absence of phytohormones perhaps along a less steep gradient (**Supplemental Figure 5A**). This suggests that H1.2 reduction may be initiated during the isolation of leaf iPSC rather than induced by culturing. Next, we interrogated the entire family of chromatin features with or without hormones, using PCA. The analysis showed that Arabidopsis iPSC cultured without hormones undergo similar changes in chromatin organisation than in the presence of hormones (**Figure 5A**, **Supplemental Figure 5B**). However, and unexpectedly, we detected that chromatin organisation heterogeneity (measured by the entropy on the LBP texture of H2B-RFP distribution) decreased significantly more in the absence of phytohormones (**Figure 5B**), whereas the heterogeneity of intensity and morphology features were not, or only moderately affected (**Supplemental Figure 5C**). We made the same observation when culturing the cells in a nutrient poor medium (W5) with or without phytohormones (**Supplemental Figure 5D**). This suggests a contribution of phytohormones to prevent homogenisation (loss of heterogeneity) in Arabidopsis iPSC cultures.

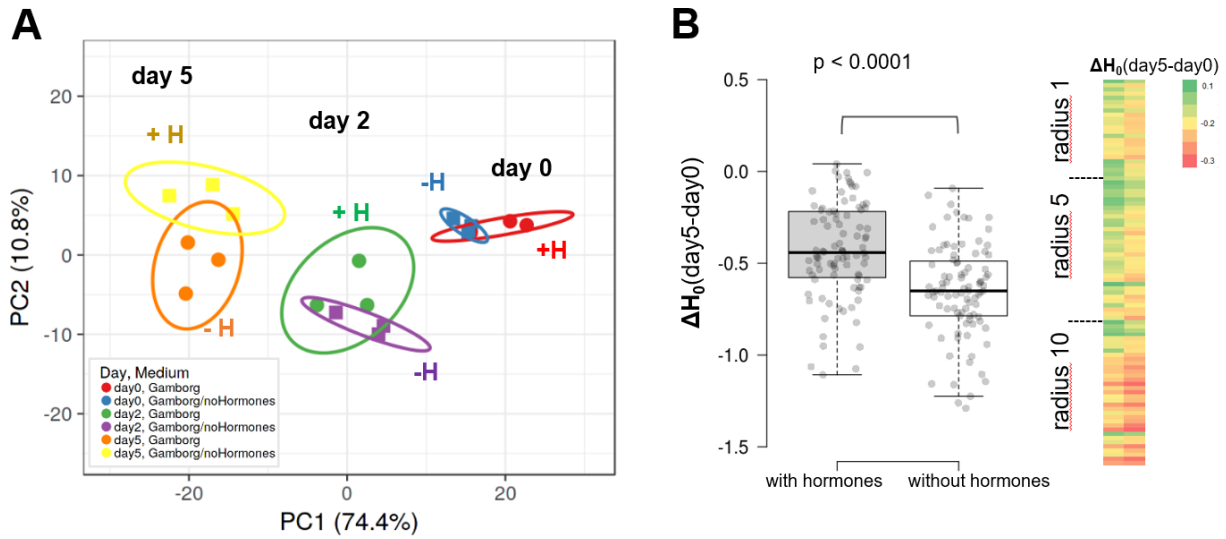

Figure 5. Phytohormones do not influence the trajectory of chromatin changes induced by culturing but dampen entropy reduction

(**A**) PCA of chromatin features of iPSC cultured in the Gamborg medium, including phytohormones ('Gamborg' or '+H' as quick annotation on the graph), or in the same basis but without phytohormones ('Gamborg/no Hormones' or '-H' as quick annotation on the graph). The PCA was computed with all features (see Methods, experiment HTI004). (**B**) Differential entropy (ΔH_0) between day 5 and day 0 for the chromatin texture features (LBP texture metrics, H2B-RFP) of iPSC cultured in Gamborg with or without hormones as indicated.

Nutrient availability influence chromatin changes during culturing.

To answer the question whether chromatin changes respond to the physiological quality of the medium we partitioned a pool of freshly released leaf iPSC into W5 (nutrient poor, (Yoo et al.,

2007)) or Gamborg B5 (nutrient rich, (Gamborg et al., 1968)), both prepared with or without phytohormones (see **Supplemental Table 2**). We analysed the chromatin features as before focusing on the first two days. Clearly, the culturing medium strongly influenced the chromatin changes with distinct trajectories principally influenced by the nutrient basis more than by the phytohormones (**Figure 6A**, **Supplemental Figure 6A**).

Next, to verify whether the nutrient composition influences chromatin changes further in time we imaged new leaf iPSC cultures for seven days. The analysis confirmed that major changes occur essentially between day 0 and day 3, yet according to different trajectories depending on the medium, and with chromatin features stabilising rapidly after day 3 (**Supplemental Figure 6B**). The typical process of H1.2 reduction also occurred in the nutrient poor medium (W5) although at a slightly lower rate (**Supplemental Figure 6C**). The medium affected nuclei morphology (**Figure 6B, Supplemental Figure 6D**) with notably rounder and larger nuclei in the nutrient poor (W5) medium (**Figure 6C, Supplemental Figure 6D-E**). The nutrient poor medium also dampened changes in chromatin texture across all length scales possibly indicating a slower transition in chromatin reorganisation (**Figure 6E**).

Finally, we asked whether, the heterogeneity of chromatin features may be affected by the culturing medium. The differential entropy (ΔH_0) between day 0 and day 7 per family of features did not reveal an overall significant effect of the medium (**Supplemental Figure 6F**), although, some morphology features showed an increase (*eg* Area) or a decrease (*eg* Roundness) in entropy in the nutrient poor medium compared to the Gamborg's medium (**Supplemental Figure 6G**).

In conclusion, the culturing medium strongly influenced chromatin dynamics of leaf iPSC, principally within the first two (three) days. Nutrients mostly influence nuclei size and shape, and chromatin texture, with lower nutrient availability inducing rounder, bigger nuclei with a less differentiated chromatin texture.

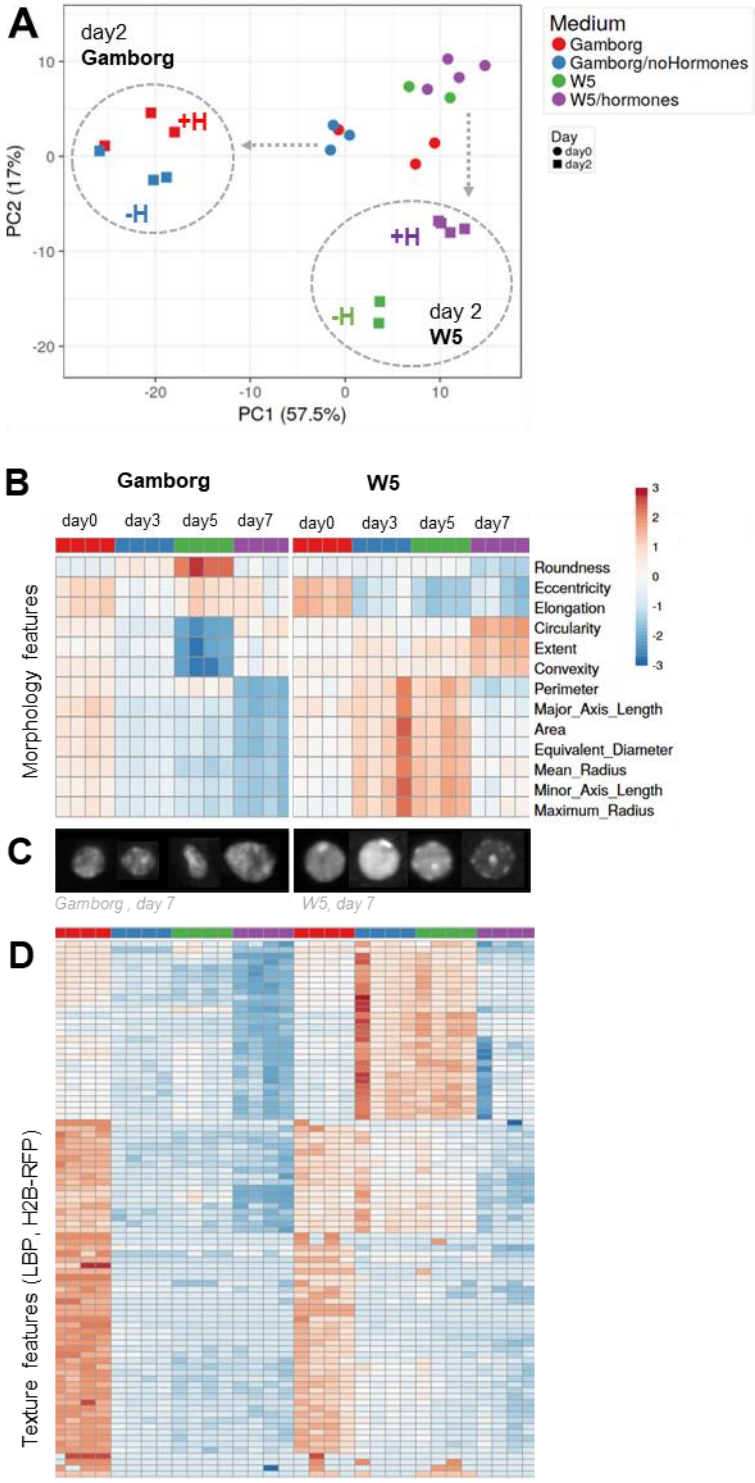

Figure 6. Nutrient availability strongly influences the trajectory of chromatin changes in iPSC cultures

(**A**) PCA of chromatin features in iPSC cultured in either a nutrient rich (Gamborg) or nutrient poor (W5) medium, each with (+H) or without (-H) hormones. The cultures stem from the same, original pool of iPSC partitioned in the different media and imaged at day 0 and day 2 in two or three replicate wells (number of datapoint with the same colour). Data from HTI004 and HTI005. (**B**) Morphological features of nuclei from iPSC cultured in either Gamborg or W5, at day 0, 3,5 and 7 (HTI001), each square unit is a replicate well. Median values are normalised (centred by rows) and the colour scale shows the fold change. (**C**) Representative nuclei of the same experiment, day 7. (**D**) Chromatin texture features (LBP method, H2B-RFP signal) of the same cultures as in B showing comparatively stronger changes between day 0 and day 2 in Gamborg compared to in W5.

Trichostatin A (TSA), an inhibitor of histone deacetylation increases heterogeneity of chromatin patterns.

Next, we tested the influence of Trichostatin A, a compound known to inhibit histone deacetylases and increase histone acetylation (Yoshida et al., 1995). TSA treatment was shown to enhance the regenerative competence of lettuce and nicotiana iPSC cultures, notably inducing a higher rate of division starting from day 5 (Choi et al., 2023). We rationalised that this drug could possibly accelerate chromatin decondensation or create changes in chromatin features detectable with our approach. First, a global analysis using PCA did not reveal a major influence of TSA (**Supplemental Figure 7A**). Also, TSA did not prevent nor accelerate H1.2 reduction, a typical event of the first culturing day, yet maintained a small fraction of cells with a high H1.2:H2B ratio at day 5 (**Supplemental Figure 7B**). The treatment also moderately influenced nuclei size (**Supplemental Figure 7C**) but not shape. Possibly, chromatin acetylation as described earlier in tobacco iPSC (Williams et al., 2003) is so rapid that TSA may act redundantly. However, when we measured the entropy of chromatin features, and more specifically the differential entropy between day 5 and day 0, we observed a strong effect of the treatment Indeed, TSA abolished or strongly diminished the differential entropy for most features (**Figure 7A**), indicating that iPSC maintained a high level of heterogeneity at day 5. Hence, histone deacetylation may contribute to channel chromatin reorganisation during the first days of culturing.

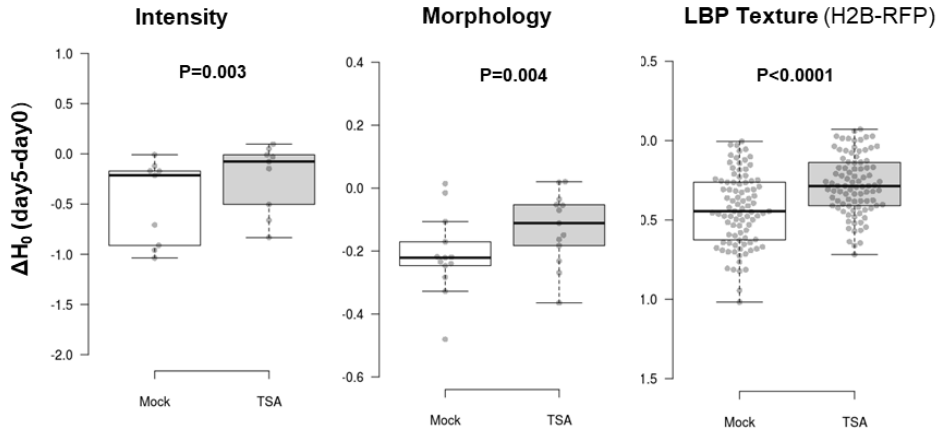

Figure 7. TSA prevents entropy reduction of iPSC chromatin features

Differential entropy (ΔH_0) between day 5 and day 0 for families of chromatin features as indicated, comparing iPSC cultured in the Mock medium (Gamborg complemented with 2% DMSO) or in the same medium supplemented with 200nM TSA in DMSO. Dataset HTI004.

Discussion

Plant iPSC cultures, also commonly called protoplast cultures, offer numerous applications in biotechnology (Reed & Bargmann, 2021). They also provide an attractive model to study transdifferentiation although not all cells share the same potential (Pasternak et al., 2020; Sugimoto et al., 2011). For instance, in a leaf-derived iPSC culture the number of cells showing a regenerative potential can be as low as 0.5% (Xu et al., 2022). Yet, globally, the culture undergoes an extensive transcriptome reprogramming and large-scale chromatin reorganisation (Chupeau et al., 2013; Moricova et al., 2013; Tessadori et al., 2007; Williams et al., 2003; Xu et al., 2021; Zhao et al., 2001). Yet, even in a relatively homogenous culture as that of leaf-derived iPSC composed of 85% mesophyll cells, gene expression changes appear largely stochastic (Xu et al., 2022), hence raising the question of the level of heterogeneity and its role in plant iPSC cultures.

We therefore established and validated a semi-automated pipeline for high-throughput quantitative analysis of chromatin reporters at the single cell level, allowing a detailed analysis of the level of heterogeneity controlled by the culturing environment and intrinsic epigenetic controls during plant iPSC generation.

Harnessing the informative potential of image features provide a new perspective on chromatin organisation in plant iPSC.

Semi-automated high throughput imaging, followed by supervised image segmentation allowed us to record several hundreds of nuclei per day of observation, in 2-4 replicate cultures per experiment. Image analysis computed by Tissue Maps (http://tissuemaps.org/index.html) returned three family of features describing chromatin organisation: Morphology descriptors of nucleus size and shape (the nucleus is the segmented object based on the H2B-RFP signal); Intensity variables for each of the two, jointly expressed, chromatin markers consisting of fluorescently labelled histones H2B and H1.2, respectively; and texture descriptors of the chromatin markers' distribution.

Morphology and intensity features are commonly used to describe characteristics of segmented cells or nuclei because they are intuitive. Beyond the size, shape descriptors inform here on the roundness, elongation, convexity or solidity of the nuclei, which can be apprehended collectively in a multivariate analysis. Intensity features, in addition, inform on the absolute levels of each chromatin markers (intensity sum), their global compactness or density in the nucleus (intensity mean) and their intensity variability in the segmented object (standard deviation, minima and

maxima). By contrast, texture features give abstract representations of signal distribution that cannot intuitively be assigned to a particular distribution pattern, *i.e.* a chromatin phenotype in our case. Yet, those are useful to identify structured and repeated patterns (Depeursinge et al., 2017b; Di Cataldo & Ficarra, 2017). Here, we focused on the LBP method (Local Binary Pattern) that compute a local representation of signal distribution, based on pixel neighbourhood analysis, along circles of incrementally bigger radius, and scanning a growing number of positions along each circle (Ojala et al., 2001). The higher the LBP values at a given radius the more heterogeneous the signal distribution, hence informing on chromatin structures with contrasted density, at different length scales. This approach was reported to be powerful to classify the chromatin types from healthy vs carcinogenic cells presenting different aggregation phenotypes (Priyanka Rana et al., 2021; Venkatachalapathy et al., 2021). Texture analysis indirectly informs on the homogeneity vs aggregation of chromatin at the mesoscale (determined by the LBP method scanning along window of different pixel size) and conceivably also capture the relative proportions of interchromatin compartment (Cremer et al., 2020). This approach thus nicely complements former cytological observations describing the disaggregation of the, relatively large-scale, heterochromatin domains at day 0 and their progressive reassembly (Ondřej et al., 2009; Tessadori et al., 2007; Williams et al., 2003; Zhao et al., 2001). We confirmed here that texture features allowed to capture changes in iPSC chromatin organisation at different length scales (see below).

A rapid, multiscale reorganisation of chromatin which trajectory depends on nutrient availability and less on phytohormones.

The release of iPSC from plant tissues induces dramatic chromatin disorganisation, with the disassembly of heterochromatin domains being a landmark confirmed in different species (Ondřej et al., 2009; Ondrej et al., 2010; Tessadori et al., 2007; Williams et al., 2003; Xu et al., 2021; Zhao et al., 2001). Culturing induces a progressive reassembly of heterochromatin domains and re-entry in the cell cycle (starting day 4 and beyond) in the presence of phytohormones (Tessadori et al., 2007; Williams et al., 2003; Xu et al., 2021; Zhao et al., 2001). Here, high throughput imaging allowed to capture additional characteristics of chromatin dynamics in particularly heterogenous iPSC cultures and the role of culturing media. Multivariate analysis identified a clear shift in chromatin features between day 0 and day 2-3, both when considering all or each family of features (morphology, intensity and textures) separately. This indicates that chromatin reorganisation occurs at multiple scale. Specifically, leaf-derived iPSC harbour changes in nuclear morphology, in H1.2 and H2B intensities levels and distribution and in chromatin texture. The

pronounced, decreased abundance of both H1.1 and H1.2 suggest large-scale changes in chromatin composition which may explain the enhanced chromatin accessibility (Xu et al., 2021; Zhao et al., 2001). Yet, interestingly, while reduced H1 levels would be expected to correlate with chromatin decompaction and increased nuclear size (Rutowicz et al., 2019), this was not the case in leaf-derived iPSC. This suggests additional mechanisms controlling nuclear size counteracting chromatin decondensation. In Arabidopsis, H1 abundance largely influence the levels and genomic distribution of DNA methylation, H3K27me3 and H3K4me3 (Rutowicz et al., 2019; Rutowicz et al., 2015; Teano et al., 2023; Wierzbicki & Jerzmanowski, 2005; Zemach et al., 2013). Whether the decrease of H1 level in iPSC chromatin triggers vast epigenomic changes could therefore be expected. Consistently, DNA methylation levels decreased -although moderately- in *Cucumis sativus* iPSC cultures (Cápal & Ondřej, 2014). Yet, a comprehensive epigenome of plant iPSC remains to be established, ideally with single cell technologies to account for the high heterogeneity.

Strikingly, nutrients availability, more than the phytohormones had an influence on the trajectory of chromatin changes. Nutrient mostly affected nuclear morphology and chromatin textures, with H1.2 reduction being largely unaffected. Low nutrient availability prevents iPSC to re-enter the cell cycle and eventually lead to cell death upon prolonged culturing (Zhao et al., 2001). Here we show that low nutrient availability has an immediate effect and led to larger, rounder nuclei with a less structured chromatin, *i.e.* displaying low textures, even until day 5-7. This is reminiscent of the situation in animal iPSC where nutrients have a profound impact on chromatin dynamics during cellular reprogramming (Apostolou & Hochedlinger, 2013; Lu et al., 2021). Metabolic fluxes are thought to influence the availability of metabolites used in epigenomic modifications both in plant and animal cells (Apostolou & Hochedlinger, 2013; Lindermayr et al., 2020; Lu et al., 2021; Lu et al., 2023), up to the point where energy metabolism was shown to influence cell fate decisions (Ly et al., 2020). Here, the nutrient rich and nutrient poor media differed not only in the amount of micro- and macronutrients but also in sugar availability. Glucose levels have been shown to control, via the TOR signalling pathway, the cytoplasmic-to-nuclear ratio of *Polycomb*-group repressive complex 2 (PRC2) components influencing H3K27me3 deposition (Ye et al., 2022). H3K27me3 reprogramming is essential for the acquisition of pluripotency in tissue explants primed for callus development *in vitro* (He et al., 2012). Given the ground role of H3K27me3 in cell identity and pluripotency in multicellular organisms, it is tempting to speculate that iPSC may undergo H3K27me3 reprogramming within the first culturing days, under the joint influence of H1, (Rutowicz et al., 2019; She et al., 2013; Teano et al., 2023) and sugar/nutrient availability (Lu et

al., 2023; Ye et al., 2022). Whether other nutrients influence iPSC chromatin organisation is nevertheless likely given the dramatic impact of nutrient availability on the trajectories of chromatin features.

iPSC chromatin features show a high entropy which reduces over time and is antagonistically by phytohormones and histone deacetylation.

Transcriptome analyses of iPSC cultures from different plant species, have shown extensive reprogramming compared to the source tissue (Cápal & Ondřej, 2014; Chupeau et al., 2013; Xu et al., 2021). Yet recently, single cell-based reconstructions demonstrated a high heterogeneity of transcriptome patterns even in a relatively homogenous plant iPSC culture consisting in 85% mesophyll cells (Xu et al., 2021). Cell-to-cell variability, particularly in animal system, has been recognized as an important factor controlling the inherent properties of a cellular system prompting investigations to understand its origin and regulation (Eldar & Elowitz, 2010; Eling et al., 2019; Guillemin & Stumpf, 2021; Huang, 2009; Mitchell & Hoffmann, 2018; Mojtahedi et al., 2016; Pelkmans, 2012; Richard & Yvert, 2014; Safdari et al., 2020). One approach to measure the heterogeneity, or information content, of biological systems is based on the calculation of the Shannon entropy borrowed from statistical mechanics (Gandrillon et al., 2021; MacArthur & Lemischka, 2013). It has been successfully applied to measure variability vs robustness of gene expression during cell differentiation (Dussiau et al., 2022; Richard et al., 2016; Stumpf et al., 2017; Wiesner et al., 2018) and reprogramming (Guillemin et al., 2019; Ye et al., 2020). Recently as well, entropy analysis was used to describe heterogeneity of chromatin states at developmentally regulated loci, as an effective information content predicting local genome topology and the competence to binding transcription factors (D'Oliveira Albanus et al., 2021). Here, and consistent with stochastic gene expression in leaf-derived iPSC (Xu et al., 2021), we identified a high entropy of chromatin features in freshly released iPSCs. This is reminiscent of mouse and human iPSCs displaying a high level of transcriptome and epigenetic heterogeneity, thought to correlated with their functional heterogeneity (Cahan & Daley, 2013; Yokobayashi et al., 2021).

Interestingly, entropy decreases over culturing time (5-40% depending on features) suggesting a canalization process towards homogenization, although entropy remains largely positive after 5-7 days culturing. We found that entropy reduction is attenuated in the absence of phytohormones and promoted when cells are exposed to an inhibitor of histone deacetylation. In contrast, nutrient availability did not influence the heterogeneity of chromatin features. Interestingly, during erythroid cells differentiation stochasticity in gene expression was increased in the presence of a drug

inhibiting histone acetylation (Guillemin et al., 2019), rather than deacetylation as in our case. Possibly, the heterogeneity of chromatin patterns and that of transcription profiles are uncoupled to some extent, but more studies on the control of gene expression stochasticity in iPSC cultures are necessary.

Is chromatin entropy as functional determinant of plant iPSC pluripotency?

A link between chromatin dynamics and chromatin pattern heterogeneity with the actual ability of plant iPSC cultures to reprogramme remains to be established. Indeed, only a small fraction of cells from a plant iPSC culture harbour effective regenerative ability (Pasternak et al., 2020; Sugimoto et al., 2011). Interestingly, in an Arabidopsis, leaf-derived iPSC culture consisting in 85% mesophyll cells, hence a priori relatively homogenous, only 5% cells seem to contribute an effective regeneration process (Xu et al., 2021). This is reminiscent from animal iPSC cultures showing variable levels of cellular reprogramming (0.5-10%, occasionally >50%) depending on the tissue source and inductive method (Kalra et al., 2021; Romanazzo et al., 2020).

Yet, also, pluripotency in animal iPSC is argued to be an emerging property of an intrinsically entropic cellular system, rather than from a unique property at the single cell level (MacArthur & Lemischka, 2013). In this conceptual framework, where pluripotency is a statistical property of a microstate system, uncommitted PSCs undergo weak regulatory constraints leading to a high entropy and stochasticity in gene expression and chromatin states (MacArthur & Lemischka, 2013). As differentiation progresses, more regulatory constraints apply and the heterogeneity of the cellular system diminishes (MacArthur & Lemischka, 2013). Our findings suggest a similar conceptual framework to explain plant iPSC properties: while the release of cell-wall free cells away from the tissue context abolishes regulatory constraints stabilising their identity, appropriate culturing conditions progressively restore regulatory signals that exert a reduction of chromatin features entropy. Interestingly in this process, we found that phytohormones, at least the specific ratio and concentration used here, are dampening this process and nutrient availability does not affect entropy reduction. This suggests intrinsic properties of plant iPSC to re-establish regulatory constraints reducing the entropy of the cellular system.

In addition, the multiscale heterogeneity of chromatin patterns (as captured by textures) is reminiscent from the finding that variations in local chromatin density underscore the differentiation competence of hESC (human embryonic stem cells, (Golkaram et al., 2017)). This heterogeneity, which is influenced by genomic contacts but also by DNA free space in the nucleus -a variable intrinsically captured by textures in our cytological analysis - is proposed to reflect

variable states of molecular crowding, which in turn controls transcriptional bursts and noise underlying cellular reprogramming (Golkaram et al., 2016; Golkaram et al., 2017).

Our work opens new perspectives to understand cellular reprogramming and pluripotency in plant iPSC systems, notably by considering the role and the regulatory mechanisms of cell-to-cell variability and associated chromatin and transcription entropy as driving factors.

Materials & Methods

Plant material and growth conditions

The *Arabidopsis thaliana* plant lines expressing fluorescently tagged H1 variants under their native promoters were formerly described (Rutowicz et al., 2019; Rutowicz et al., 2015). To generate the dual chromatin reporter line H1.2-GFP/H2.B-RFP the line *promH1.2::H1.2-GFP* (Rutowicz et al., 2015) was crossed with *promUBQ10::H2B-RFP* (von Wangenheim et al., 2016).

Seeds were surface sterilized and rinsed in sterile water before transferring on the sterile germination medium (0.5 × MS medium, 1% agar). Seeds were placed on the medium with ca 1 cm distance using toothpicks, stratified 2 days at 4°C and grown 3 weeks in long day photoperiod (16 h, 22 °C day/8 h, 18 °C night) and light flux around 100 µM s−1 m−2.

Plant iPSC preparation and culture

Protoplasts were isolated from Arabidopsis leaves based on published protocols (Li et al., 2014; Yoo et al., 2007) with some modifications to ensure sterile conditions during isolation and protoplast culturing and described thereafter. The whole procedure was performed under the laminar hood. All solutions were filter sterilized using 0.22- µm filters. Blades, forceps, white pieces of paper, tubes were autoclaved. For pipetting the sterile filter tips were used. After leaf tissue digestion protoplasts were filtered with sterile single-use cell strainers with 70 µm pores. After isolation cells were suspended in intended media (see **Supplemental Table 2**) and distributed into coverglass-bottom, 96-well plates Greiner Bio-One, Ref: 655087 in 100 µl culture per well. The outer wells of the plate were excluded due to the limited field of view and travel range at imaging. Each plate was sealed with 3M tape to avoid drying, wrapped into a layer of aluminium foil and placed in the growth chamber for 5 to 7 days depending on the experiment.

For the Trichostatin A (TSA) treatment, 100 nM or 200 nM TSA in DMSO was added at day 0 in the culture or the equivalent amount of DMSO (2% or 4%, Mock).

To assess cell viability, fluorescein diacetate (FDA) was added at either day 0, day 2 or day 5 before imaging.

Microscopy imaging

Microscopy images of iPSCs shown in Figure 1 were taken with a laser scanning confocal microscope (Leica SP5, Leica microsystems, Germany). For scoring (graphs Figure 1) the percentage of iPSCs expressing the chromatin markers were scored manually under an epi-fluorescence microscope (Leica DM6000 Leica microsystems, Germany).

Semi-automated imaging of leaf iPSC, cultured in coverglass-bottom 96-well plates (see above) were imaged using a confocal microscope Cell Voyager (CV7000, Yokogawa), equipped with a 60x water immersion objective (Nikon, NA1.2) using a illumination by 100-200 mW lasers from Coherent (depending on the channel) and filters from Chroma. Images were acquired as 16-bit images using two Neo sCMOS cameras (Andor), pixel size 6.5 µm/M.

For each well, six regions of interest (ROI) corresponding to a field of view of 277 µm x 234 µm with an image format of 2560 x 2160 pixels over 16 z planes with a step of 1 µm. ROIs were randomly chosen without overlap. Imaging time for one well = 90 seconds; Imaging time for one plate (60 wells) = 90 minutes.

Image analysis

Images were loaded into TissueMAPS (www.tissuemaps.org, code available at https://github.com/pelkmanslab/TissueMAPS) where ROIs were grouped as 2x3 grids per well. Illumination correction based on averaged intensity statistics across all images and maximum intensity projection along the Z dimension was performed in TissueMaps.

Image processing – was done in TissueMaps v0.6.3 for the following steps: (i) gaussian smoothing with a filter-size of 5 pixels; (ii) Otsu-thresholding in a user-defined range using the red (H2B-RFP) channel, followed by binary mask filling and filtering objects < 200 pixels in area to get segmentation; (iii) feature measurements using the measure_morphology, measure_intensity and measure_texture modules in TissueMaps for both channels without the smoothing applied (see list Table 1); (iv) classification of missegmentations by interactive training of SVMs (Support Vector Machine) in TissueMAPS. For the training, two classes of objects were annotated and created: A, correctly-segmented and B, non-correctly segmented. Then for each class around 40-50 objects were labelled manually. Object morphology and RFP/GFP intensity features were chosen for training the classifier. In particular the following parameters: area, circularity,

roundness, elongation, convexity, mean intensity in RFP channel and mean intensity in GFP channel. In total, 100 objects in 10 images (total=1000) were used for training and resulted in 95% segmentation accuracy (n=417), with 4 of the 5% false positive being truncated nuclei at the edge of the image and 1% corresponding to undersegmented nuclei (**Supplemental Figure 8**). The description of the SVM algorithm which was used here is available at https://scikit-learn.org/stable/modules/svm.html). Features measurements and object classification were then downloaded from TissueMaps for further analysis. In R (Rproject.org), we further filtered away outlier nuclei with an area >5000 pixels ("giant nuclei", 1-5% per dataset, possibly from trichomes (Walker et al., 2000)).

Principal Component Analysis (PCA)

PCA were computed using Clustvis (Metsalu & Vilo, 2015). Columns with similar annotations were collapsed by taking the median inside each group. Unit variance scaling was applied to rows. SVD with imputation was used to calculate the principal components. X and Y axis show principal component 1 and principal component 2 that explain the given % of the total variance, respectively. Prediction ellipses depict a 95% confidence interval (a new observation from the same group will fall inside the ellipse with probability p=0.95).

Entropy analysis

The initial script for computing Shannon Entropy is described in DOI: 10.1186/s12915-022-01264-9 and is available at https://osf.io/9mcwg/. The adapted script for computing entropy of chromatin features is provided in **Supplemental File 1**. When all cells (segmented nuclei) express the same value for a given feature, this feature's entropy will be null. The more cell-to-cell variability for a given chromatin feature, the higher value of entropy.

Plots and statistical tests

Box plots, violin plots, scatter plots, 2D contours and histograms were created using the online tools https://chart-studio.plotly.com/, http://shiny.chemgrid.org/boxplotr/ (Spitzer et al., 2014) or own R scripts (Supplemental Figure 1 only). Statistical tests indicated in the figure legends were done using R package or using the online tool https://www.statskingdom.com/mean-tests.html.

Acknowledgements

We thank Alexis Maizel (COS Heidelberg, Germany) for the Arabidopsis lines expressing the UBQ10::H2B-RFP reporter (von Wangenheim et al., 2016), Alejandro Fonseca for computational

help in running entropy analysis, Prof. Ueli Grossniklaus and group members for insightful discussions and Prof Grossniklaus department lab managers and technicians for daily support.

Funding sources

This work was supported by Swiss National Science Foundation to CB (grant numbers: SNSF, 310030_185186, IZCOZ0_182949) and University of Zurich Forschungskredit to KR (grant number: K-74502-03-01).

References

Apostolou, E., & Hochedlinger, K. (2013). Chromatin dynamics during cellular reprogramming. *Nature, 502*(7472), 462-471.

Birnbaum, K. D., & Roudier, F. (2017). Epigenetic memory and cell fate reprogramming in plants. *Regeneration (Oxf), 4*(1), 15-20.

Cahan, P., & Daley, G. Q. (2013). Origins and implications of pluripotent stem cell variability and heterogeneity. *Nature Reviews Molecular Cell Biology, 14*(6), 357-368.

Cápal, P., & Ondřej, V. (2014). Expression and epigenetic profile of protoplast cultures (Cucumis sativus L.). *In Vitro Cellular & Developmental Biology - Plant, 50*(6), 789-794.

Choi, S. H., Ahn, W. S., Lee, M. H., Jin, D. M., Lee, A., Jie, E. Y., . . . Kim, S. W. (2023). Effects of TSA, NaB, Aza in Lactuca sativa L. protoplasts and effect of TSA in Nicotiana benthamiana protoplasts on cell division and callus formation. *PLoS One, 18*(2), e0279627.

Chupeau, M. C., Granier, F., Pichon, O., Renou, J. P., Gaudin, V., & Chupeau, Y. (2013). Characterization of the early events leading to totipotency in an Arabidopsis protoplast liquid culture by temporal transcript profiling. *Plant Cell, 25*(7), 2444-2463.

Cremer, T., Cremer, M., Hubner, B., Silahtaroglu, A., Hendzel, M., Lanctot, C., . . . Cremer, C. (2020). The Interchromatin Compartment Participates in the Structural and Functional Organization of the Cell Nucleus. *Bioessays, 42*(2), e1900132.

D'Oliveira Albanus, R., Kyono, Y., Hensley, J., Varshney, A., Orchard, P., Kitzman, J. O., & Parker, S. C. J. (2021). Chromatin information content landscapes inform transcription factor and DNA interactions. *Nat Commun, 12*(1), 1307.

Dawson, J., Pandey, S., Yu, Q., Schaub, P., Wüst, F., Moradi, A. B., . . . Welsch, R. (2022). Determination of protoplast growth properties using quantitative single-cell tracking analysis. *Plant Methods, 18*(1), 64.

Depeursinge, A., Fageot, J., & Al-Kadi, O. S. (2017a). Chapter 1 - Fundamentals of Texture Processing for Biomedical Image Analysis: A General Definition and Problem Formulation. In A. Depeursinge, O. S. Al-Kadi, & J. R. Mitchell (Eds.), *Biomedical Texture Analysis* (pp. 1-27): Academic Press.

Depeursinge, A., Fageot, J., & Al-Kadi, O. S. (2017b). Fundamentals of Texture Processing for Biomedical Image Analysis. 1-27.

Desvoyes, B., Arana-Echarri, A., Barea, M. D., & Gutierrez, C. (2020). A comprehensive fluorescent sensor for spatiotemporal cell cycle analysis in Arabidopsis. *Nat Plants, 6*(11), 1330-1334.

Di Cataldo, S., & Ficarra, E. (2017). Mining textural knowledge in biological images: Applications, methods and trends. *Comput Struct Biotechnol J, 15*, 56-67.
Dussiau, C., Boussaroque, A., Gaillard, M., Bravetti, C., Zaroili, L., Knosp, C., . . . Kosmider, O. (2022). Hematopoietic differentiation is characterized by a transient peak of entropy at a single-cell level. *BMC Biol, 20*(1), 60.
Eldar, A., & Elowitz, M. B. (2010). Functional roles for noise in genetic circuits. *Nature, 467*(7312), 167-173.
Eling, N., Morgan, M. D., & Marioni, J. C. (2019). Challenges in measuring and understanding biological noise. *Nat Rev Genet, 20*(9), 536-548.
Gamborg, O. L., Miller, R. A., & Ojima, K. (1968). Nutrient requirements of suspension cultures of soybean root cells. *Exp Cell Res, 50*(1), 151-158.
Gandrillon, O., Gaillard, M., Espinasse, T., Garnier, N. B., Dussiau, C., Kosmider, O., & Sujobert, P. (2021). Entropy as a measure of variability and stemness in single-cell transcriptomics. *Current Opinion in Systems Biology, 27*, 100348.
Golkaram, M., Hellander, S., Drawert, B., & Petzold, L. R. (2016). Macromolecular Crowding Regulates the Gene Expression Profile by Limiting Diffusion. *PLoS Comput Biol, 12*(11), e1005122.
Golkaram, M., Jang, J., Hellander, S., Kosik, K. S., & Petzold, L. R. (2017). The Role of Chromatin Density in Cell Population Heterogeneity during Stem Cell Differentiation. *Sci Rep, 7*(1), 13307.
Grafi, G., Florentin, A., Ransbotyn, V., & Morgenstern, Y. (2011). The stem cell state in plant development and in response to stress. *Front Plant Sci, 2*, 53.
Guillemin, A., Duchesne, R., Crauste, F., Gonin-Giraud, S., & Gandrillon, O. (2019). Drugs modulating stochastic gene expression affect the erythroid differentiation process. *PLoS One, 14*(11), e0225166.
Guillemin, A., & Stumpf, M. P. H. (2021). Noise and the molecular processes underlying cell fate decision-making. *Phys Biol, 18*(1), 011002.
Hamilton, N. A., Pantelic, R. S., Hanson, K., & Teasdale, R. D. (2007). Fast automated cell phenotype image classification. *BMC Bioinformatics, 8*, 110.
He, C., Chen, X., Huang, H., & Xu, L. (2012). Reprogramming of H3K27me3 is critical for acquisition of pluripotency from cultured Arabidopsis tissues. *PLoS Genet, 8*(8), e1002911.
Holstein, T. W., Hobmayer, E., & Technau, U. (2003). Cnidarians: an evolutionarily conserved model system for regeneration? *Dev Dyn, 226*(2), 257-267.
Huang, S. (2009). Non-genetic heterogeneity of cells in development: more than just noise. *Development, 136*(23), 3853-3862.
Ibanez, S., Carneros, E., Testillano, P. S., & Perez-Perez, J. M. (2020). Advances in Plant Regeneration: Shake, Rattle and Roll. *Plants (Basel), 9*(7).
Ikeuchi, M., Favero, D. S., Sakamoto, Y., Iwase, A., Coleman, D., Rymen, B., & Sugimoto, K. (2019). Molecular Mechanisms of Plant Regeneration. *Annual Review of Plant Biology, 70*(1), 377-406.
Ishihara, H., Sugimoto, K., Tarr, P. T., Temman, H., Kadokura, S., Inui, Y., . . . Matsunaga, S. (2019). Primed histone demethylation regulates shoot regenerative competency. *Nat Commun, 10*(1), 1786.
Iwafuchi-Doi, M., & Zaret, K. S. (2014). Pioneer transcription factors in cell reprogramming. *Genes Dev, 28*(24), 2679-2692.
Iwase, A., Harashima, H., Ikeuchi, M., Rymen, B., Ohnuma, M., Komaki, S., . . . Sugimoto, K. (2017). WIND1 Promotes Shoot Regeneration through Transcriptional Activation of ENHANCER OF SHOOT REGENERATION1 in Arabidopsis. *Plant Cell, 29*(1), 54-69.

Iwase, A., Mitsuda, N., Koyama, T., Hiratsu, K., Kojima, M., Arai, T., . . . Ohme-Takagi, M. (2011). The AP2/ERF transcription factor WIND1 controls cell dedifferentiation in Arabidopsis. *Curr Biol, 21*(6), 508-514.

Jin, R., Klasfeld, S., Zhu, Y., Fernandez Garcia, M., Xiao, J., Han, S. K., . . . Wagner, D. (2021). LEAFY is a pioneer transcription factor and licenses cell reprogramming to floral fate. *Nat Commun, 12*(1), 626.

Jing, T., Ardiansyah, R., Xu, Q., Xing, Q., & Muller-Xing, R. (2020). Reprogramming of Cell Fate During Root Regeneration by Transcriptional and Epigenetic Networks. *Front Plant Sci, 11*, 317.

Kalra, R. S., Dhanjal, J. K., Das, M., Singh, B., & Naithani, R. (2021). Cell Transdifferentiation and Reprogramming in Disease Modeling: Insights into the Neuronal and Cardiac Disease Models and Current Translational Strategies. *Cells, 10*(10).

Kerr, E., Kiyuna, T., Boyle, S., Saito, A., Thomas, J. S., & Bickmore, W. A. (2010). Changes in chromatin structure during processing of wax-embedded tissue sections. *Chromosome Res, 18*(6), 677-688.

Kotlinski, M., Rutowicz, K., Knizewski, L., Palusinski, A., Oledzki, J., Fogtman, A., . . . Jerzmanowski, A. (2016). Histone H1 Variants in Arabidopsis Are Subject to Numerous Post-Translational Modifications, Both Conserved and Previously Unknown in Histones, Suggesting Complex Functions of H1 in Plants. *PLoS One, 11*(1), e0147908.

Lee, H. K., Kim, C. H., Bhattacharjee, S., Park, H. G., Prakash, D., & Choi, H. K. (2021). A Paradigm Shift in Nuclear Chromatin Interpretation: From Qualitative Intuitive Recognition to Quantitative Texture Analysis of Breast Cancer Cell Nuclei. *Cytometry A, 99*(7), 698-706.

Lee, K., & Seo, P. J. (2018). Dynamic Epigenetic Changes during Plant Regeneration. *Trends Plant Sci, 23*(3), 235-247.

Li, J. F., Zhang, D., & Sheen, J. (2014). Epitope-tagged protein-based artificial miRNA screens for optimized gene silencing in plants. *Nat Protoc, 9*(4), 939-949.

Lindermayr, C., Rudolf, E. E., Durner, J., & Groth, M. (2020). Interactions between metabolism and chromatin in plant models. *Mol Metab, 38*, 100951.

Lu, V., Roy, I. J., & Teitell, M. A. (2021). Nutrients in the fate of pluripotent stem cells. *Cell Metabolism, 33*(11), 2108-2121.

Lu, Y., Bu, Q., Chuan, M., Cui, X., Zhao, Y., & Zhou, D. X. (2023). Metabolic regulation of the plant epigenome. *Plant J*.

Ly, C. H., Lynch, G. S., & Ryall, J. G. (2020). A Metabolic Roadmap for Somatic Stem Cell Fate. *Cell Metab, 31*(6), 1052-1067.

MacArthur, B. D., & Lemischka, I. R. (2013). Statistical mechanics of pluripotency. *Cell, 154*(3), 484-489.

Metsalu, T., & Vilo, J. (2015). ClustVis: a web tool for visualizing clustering of multivariate data using Principal Component Analysis and heatmap. *Nucleic Acids Res, 43*(W1), W566-570.

Mitchell, S., & Hoffmann, A. (2018). Identifying Noise Sources governing cell-to-cell variability. *Curr Opin Syst Biol, 8*, 39-45.

Mojtahedi, M., Skupin, A., Zhou, J., Castano, I. G., Leong-Quong, R. Y., Chang, H., . . . Huang, S. (2016). Cell Fate Decision as High-Dimensional Critical State Transition. *PLoS Biol, 14*(12), e2000640.

Moricova, P., Ondrej, V., Navratilova, B., & Luhova, L. (2013). Changes of DNA methylation and hydroxymethylation in plant protoplast cultures. *Acta Biochim Pol, 60*(1), 33-36.

Muller-Xing, R., & Xing, Q. (2022). The plant stem-cell niche and pluripotency: 15 years of an epigenetic perspective. *Front Plant Sci, 13*, 1018559.

Ojala, T., Pietikäinen, M., & Mäenpää, T. (2001, 2001//). *A Generalized Local Binary Pattern Operator for Multiresolution Gray Scale and Rotation Invariant Texture Classification.*

Paper presented at the Advances in Pattern Recognition — ICAPR 2001, Berlin, Heidelberg.
Ondřej, V., Kitner, M., Doležalová, I., Nádvorník, P., Navrátilová, B., & Lebeda, A. (2009). Chromatin structural rearrangement during dedifferentiation of protoplasts of Cucumis sativus L. *Molecules and Cells, 27*(4), 443-447.
Ondrej, V., Navrátilová, B., Protivánková, I., Piterková, J., Sedlárová, M., Luhová, L., & Lebeda, A. (2010). Recondensation level of repetitive sequences in the plant protoplast nucleus is limited by oxidative stress. *J Exp Bot, 61*(9), 2395-2401.
Pasternak, T., Lystvan, K., Betekhtin, A., & Hasterok, R. (2020). From Single Cell to Plants: Mesophyll Protoplasts as a Versatile System for Investigating Plant Cell Reprogramming. *International Journal of Molecular Sciences, 21*(12). Retrieved from doi:10.3390/ijms21124195
Pelkmans, L. (2012). Cell Biology. Using cell-to-cell variability--a new era in molecular biology. *Science, 336*(6080), 425-426.
Rana, P., Sowmya, A., Meijering, E., & Song, Y. (2021). Estimation of three-dimensional chromatin morphology for nuclear classification and characterisation. *Sci Rep, 11*(1), 3364.
Rana, P., Sowmya, A., Meijering, E., & Song, Y. (2021). Estimation of three-dimensional chromatin morphology for nuclear classification and characterisation. *Sci Rep, 11*(1), 3364.
Reddy, P., Memczak, S., & Izpisua Belmonte, J. C. (2021). Unlocking Tissue Regenerative Potential by Epigenetic Reprogramming. *Cell Stem Cell, 28*(1), 5-7.
Reed, K. M., & Bargmann, B. O. R. (2021). Protoplast Regeneration and Its Use in New Plant Breeding Technologies. *Front Genome Ed, 3*, 734951.
Richard, A., Boullu, L., Herbach, U., Bonnafoux, A., Morin, V., Vallin, E., . . . Gandrillon, O. (2016). Single-Cell-Based Analysis Highlights a Surge in Cell-to-Cell Molecular Variability Preceding Irreversible Commitment in a Differentiation Process. *PLoS Biol, 14*(12), e1002585.
Richard, M., & Yvert, G. (2014). How does evolution tune biological noise? *Front Genet, 5*, 374.
Romanazzo, S., Lin, K., Srivastava, P., & Kilian, K. A. (2020). Targeting cell plasticity for regeneration: From in vitro to in vivo reprogramming. *Advanced Drug Delivery Reviews, 161-162*, 124-144.
Rutowicz, K., Lirski, M., Mermaz, B., Teano, G., Schubert, J., Mestiri, I., . . . Baroux, C. (2019). Linker histones are fine-scale chromatin architects modulating developmental decisions in Arabidopsis. *Genome Biol, 20*(1), 157.
Rutowicz, K., Puzio, M., Halibart-Puzio, J., Lirski, M., Kotlinski, M., Kroten, M. A., . . . Jerzmanowski, A. (2015). A Specialized Histone H1 Variant Is Required for Adaptive Responses to Complex Abiotic Stress and Related DNA Methylation in Arabidopsis. *Plant Physiol, 169*(3), 2080-2101.
Safdari, H., Kalirad, A., Picioreanu, C., Tusserkani, R., Goliaei, B., & Sadeghi, M. (2020). Noise-driven cell differentiation and the emergence of spatiotemporal patterns. *PLoS One, 15*(4), e0232060.
Sang, Y. L., Cheng, Z. J., & Zhang, X. S. (2018). iPSCs: A Comparison between Animals and Plants. *Trends in Plant Science, 23*(8), 660-666.
Saruyama, N., Sakakura, Y., Asano, T., Nishiuchi, T., Sasamoto, H., & Kodama, H. (2013). Quantification of metabolic activity of cultured plant cells by vital staining with fluorescein diacetate. *Anal Biochem, 441*(1), 58-62.
She, W., Grimanelli, D., Rutowicz, K., Whitehead, M. W., Puzio, M., Kotlinski, M., . . . Baroux, C. (2013). Chromatin reprogramming during the somatic-to-reproductive cell fate transition in plants. *Development, 140*(19), 4008-4019.

Shemer, O., Landau, U., Candela, H., Zemach, A., & Eshed Williams, L. (2015). Competency for shoot regeneration from Arabidopsis root explants is regulated by DNA methylation. *Plant Sci, 238*, 251-261.

Special Issue "New Frontiers in Micropropagation". (2021). https://www.mdpi.com/journal/agronomy/special_issues/micropropagation.

Spitzer, M., Wildenhain, J., Rappsilber, J., & Tyers, M. (2014). BoxPlotR: a web tool for generation of box plots. *Nat Methods, 11*(2), 121-122.

Stumpf, P. S., Smith, R. C. G., Lenz, M., Schuppert, A., Muller, F. J., Babtie, A., . . . MacArthur, B. D. (2017). Stem Cell Differentiation as a Non-Markov Stochastic Process. *Cell Syst, 5*(3), 268-282 e267.

Sugimoto, K., Gordon, S. P., & Meyerowitz, E. M. (2011). Regeneration in plants and animals: dedifferentiation, transdifferentiation, or just differentiation? *Trends in Cell Biology, 21*(4), 212-218.

Teano, G., Concia, L., Carron, L., Wolff, L., Adamusová, K., Fojtová, M., . . . Barneche, F. (2023). Histone H1 protects telomeric repeats from H3K27me3 invasion in Arabidopsis. *Cell Reports, In press*.

Tessadori, F., Chupeau, M. C., Chupeau, Y., Knip, M., Germann, S., van Driel, R., . . . Gaudin, V. (2007). Large-scale dissociation and sequential reassembly of pericentric heterochromatin in dedifferentiated Arabidopsis cells. *J Cell Sci, 120*(Pt 7), 1200-1208.

Venkatachalapathy, S., Jokhun, D. S., Andhari, M., & Shivashankar, G. V. (2021). Single cell imaging-based chromatin biomarkers for tumor progression. *Sci Rep, 11*(1), 23041.

von Wangenheim, D., Fangerau, J., Schmitz, A., Smith, R. S., Leitte, H., Stelzer, E. H., & Maizel, A. (2016). Rules and Self-Organizing Properties of Post-embryonic Plant Organ Cell Division Patterns. *Curr Biol, 26*(4), 439-449.

Walker, J., Oppenheimer, D., Concienne, J., & Larkin, J. (2000). SIAMESE, a gene controlling the endoreduplication cell cycle in Arabidopsis thaliana trichomes. *Development (Cambridge, England), 127*, 3931-3940.

Wierzbicki, A. T., & Jerzmanowski, A. (2005). Suppression of histone H1 genes in Arabidopsis results in heritable developmental defects and stochastic changes in DNA methylation. *Genetics, 169*(2), 997-1008.

Wiesner, K., Teles, J., Hartnor, M., & Peterson, C. (2018). Haematopoietic stem cells: entropic landscapes of differentiation. *Interface Focus, 8*(6), 20180040.

Williams, L., Zhao, J., Morozova, N., Li, Y., Avivi, Y., & Grafi, G. (2003). Chromatin reorganization accompanying cellular dedifferentiation is associated with modifications of histone H3, redistribution of HP1, and activation of E2F-target genes. *Dev Dyn, 228*(1), 113-120.

Xu, M., Du, Q., Tian, C., Wang, Y., & Jiao, Y. (2021). Stochastic gene expression drives mesophyll protoplast regeneration. *Sci Adv, 7*(33).

Xu, Y., Li, R., Luo, H., Wang, Z., Li, M.-W., Lam, H.-M., & Huang, C. (2022). Protoplasts: small cells with big roles in plant biology. *Trends in Plant Science, 27*(8), 828-829.

Ye, R., Wang, M., Du, H., Chhajed, S., Koh, J., Liu, K. H., . . . Sheen, J. (2022). Glucose-driven TOR-FIE-PRC2 signalling controls plant development. *Nature, 609*(7929), 986-993.

Ye, Y., Yang, Z., Zhu, M., & Lei, J. (2020). Using single-cell entropy to describe the dynamics of reprogramming and differentiation of induced pluripotent stem cells. *International Journal of Modern Physics B, 34*(30), 2050288.

Yokobayashi, S., Yabuta, Y., Nakagawa, M., Okita, K., Hu, B., Murase, Y., . . . Saitou, M. (2021). Inherent genomic properties underlie the epigenomic heterogeneity of human induced pluripotent stem cells. *Cell Reports, 37*(5), 109909.

Yoo, S. D., Cho, Y. H., & Sheen, J. (2007). Arabidopsis mesophyll protoplasts: a versatile cell system for transient gene expression analysis. *Nat Protoc, 2*(7), 1565-1572.

Yoshida, M., Horinouchi, S., & Beppu, T. (1995). Trichostatin A and trapoxin: novel chemical probes for the role of histone acetylation in chromatin structure and function. *Bioessays, 17*(5), 423-430.

Zemach, A., Kim, M. Y., Hsieh, P. H., Coleman-Derr, D., Eshed-Williams, L., Thao, K., . . . Zilberman, D. (2013). The Arabidopsis nucleosome remodeler DDM1 allows DNA methyltransferases to access H1-containing heterochromatin. *Cell, 153*(1), 193-205.

Zhao, J., Morozova, N., Williams, L., Libs, L., Avivi, Y., & Grafi, G. (2001). Two phases of chromatin decondensation during dedifferentiation of plant cells: distinction between competence for cell fate switch and a commitment for S phase. *J Biol Chem, 276*(25), 22772-22778.